Chemoresponsive monolayer transistors

Xuefeng Guo*†, Matthew Myers*†, Shengxiong Xiao*†, Michael Lefenfeld*†, Rachel Steiner†‡, George S. Tulevski*†, Jinyao Tang*†, Julian Baumert§, Frank Leibfarth*†, James T. Yardley†¶, Michael L. Steigerwald*†, Philip Kim†‖, and Colin Nuckolls*†**

Departments of *Chemistry, ‖Physics, ‡Applied Physics/Applied Mathematics, and ¶Electrical Engineering, and †Columbia University Center for Electronics of Molecular Nanostructures, Columbia University, New York, NY 10027; and §Condensed Matter Physics and Materials Science, Brookhaven National Laboratory, Upton, NY 11973

Edited by Harry B. Gray, California Institute of Technology, Pasadena, CA, and approved June 9, 2006 (received for review March 1, 2006)

This work details a method to make efficacious field-effect transistors from monolayers of polycyclic aromatic hydrocarbons that are able to sense and respond to their chemical environment. The molecules used in this study are functionalized so that they assemble laterally into columns and attach themselves to the silicon oxide surface of a silicon wafer. To measure the electrical properties of these monolayers, we use ultrasmall point contacts that are separated by only a few nanometers as the source and drain electrodes. These contacts are formed through an oxidative cutting of an individual metallic single-walled carbon nanotube that is held between macroscopic metal leads. The molecules assemble in the gap and form transistors with large current modulation and high gate efficiency. Because these devices are formed from an individual stack of molecules, their electrical properties change significantly when exposed to electron-deficient molecules such as tetracyanoquinodimethane (TCNQ), forming the basis for new types of environmental and molecular sensors.

chemistry | electronic materials | nanoscience | self-assembly

This work details a method to make chemoresponsive transistors by making devices out of a monolayer of polycyclic aromatic hydrocarbons that are chemically attached to surfaces. The devices are formed through a self-assembly process of organic semiconductors on the oxide surface of a silicon wafer (Fig. 1*A*) (1, 2). Previous studies on organic field-effect transistors (OFETs) (3, 4) have shown that the path for electrical current is through at most the first few layers of molecules at the oxide interface (5–7). In general, when the semiconducting layers of typical OFETs are scaled down to a monolayer, their properties become poor, presumably due to discontinuities or defects in the films (8–11). The strategy used here circumvents this problem by a chemical functionalization of the molecular semiconductors (Fig. *1B*) so that they both assemble laterally and chemically attach themselves to the substrate (Fig. 1*C*). The important result is that when ultrasmall point contacts separated by molecular length-scales are used as the source and drain (S/D) electrodes, transistors can be made that have high gate efficiency and large ON/OFF ratios from only a monolayer of molecules. The electrical properties of these monolayers are responsive to electron acceptors such as tetracyanoquinodimethane (TCNQ).

Results and Discussion

Device Fabrication. We first describe the devices used to measure the properties of the monolayers and then the structural and electrical characterization of these monolayers. Fig. 2 shows a schematic and micrograph of the devices used. Au (50 nm) on Cr (5 nm) pads, which are separated by 20 μm, form the contact to an individual single-walled carbon nanotube (SWNT). The nanotubes were grown by a chemical vapor deposition (CVD) process described elsewhere (12, 13). The nanotube is then oxidatively cut by using an ultrafine lithographic process that produces a very small gap between the nanotube ends (13–15). In a previous study, we measured the distance between the tubes by covalently bridging them with molecules and found the separation to be between 2 and 6 nm (13). It is in this gap that we intend to self-assemble monolayers of organic semiconductors. By applying a S/D bias voltage (V_D) to the metal electrodes attached to the nanotubes and measuring drain current I_D, these gaps allow us to probe the electrical conduction through small collections of molecules whose properties have not been degraded by grain boundaries or defects (14, 15). The doped silicon wafer acts as the global gate electrode and by applying gate bias voltage (V_G), we can tune the carrier density in the devices (16–18).

Investigating the I_D vs. V_G characteristics, we screen the current–voltage characteristics of the SWNT devices before cutting and categorize them as metallic ($|I_D| > 0$, for all V_G) or as a *p*-type semiconductor ($I_D = 0$, for $V_G > V_{th}$, where V_{th} is the threshold voltage). To aid in the subsequent analysis of the devices, we only use those that are formed from metallic SWNTs. Fig. 2*C* compares the electrical properties of a metallic SWNT before and after it is cut. Before cutting, the resistance of the device is $\approx$0.8 MΩ, and after cutting the circuit is now open with the current of the device at the noise limit of the measurement ($\approx$2 pA).

Monolayer Formation. We next turn our attention to the preparation of the functionalized organic semiconductors and their assembly on the surface of silicon oxide. We used the contorted hexabenzocoronenes (Fig. 1*B*) because we have shown previously that compound **1A,** which is surrounded by four alkyl groups, self-organizes into molecular stacks with exceptional semiconducting properties (19). Moreover, these molecules are extremely stable in ambient conditions. For this study, we designed derivatives of **1A** that present carboxylic acid substituents on one of its edges because this functionality is well known to bind to the surface of silicon oxide (20–22). Their syntheses are detailed in Scheme 1, which is published as supporting information on the PNAS web site. Owing to their low solubility, we found it extremely difficult to form monolayer films with the acids, but the acid chlorides (**1B** and **1C**), which are readily soluble in common organic solvents, easily form high-coverage monolayers on silicon oxide. By using the optical molar extinction coefficient (8×10^4 $M^{-1}\cdot cm^{-1}$ in THF solution), we estimated its coverage on quartz windows to be $\approx$0.7 molecules in a 1×1-nm square for both **1B** and **1C**. This estimation is in reasonable agreement with the 0.9 molecules per nm^2 estimated for a disk that is upright on the surface and close-packed into columns (see Fig. 6, which is published as supporting information on the PNAS web site).

The surface reaction between the carbonyl chlorides of the

Conflict of interest statement: No conflicts declared.

This paper was submitted directly (Track II) to the PNAS office.

Abbreviations: SWNT, single-walled carbon nanotube; OFET, organic field-effect transistor; HBC, hexa-kata-benzocoronene; S/D, source and drain; TCNQ, tetracyanoquinodimethane; UV-vis, UV-visible.

**To whom correspondence should be addressed. E-mail: cn37@columbia.edu.

www.pnas.org/cgi/doi/10.1073/pnas.0601675103

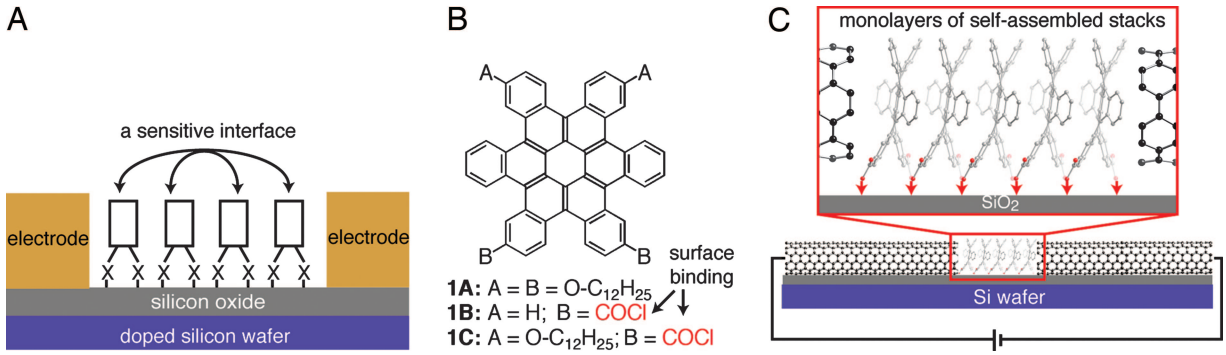

Fig. 1. A schematic of how HBCs can be formed into a monolayer and measured with ultrasmall point contacts. (*A*) An alternative molecular electronics where molecules are attached through the X-group to a primer layer for assembly and probed laterally. The semiconductor/air interface should be very sensitive to its environment. (*B*) HBC molecules. **1A** assembles into 1D stacks. **1B** and **1C** synthesized with groups to bind them to the surface of silicon oxide. (*C*) Monolayers of self-assembled stacks being probed with SWNT electrodes separated by only a few nanometers.

hexabenzocoronenes and the oxygens of the silicon oxide produces an ester. After reaction of **1B** and **1C** with a silicon wafer, their IR spectrum (Fig. 3*A*) shows the loss of its acid chloride C═O stretch (1,751 cm^{-1}) and appearance of a new carbonyl stretch at 1,740 cm^{-1}. This frequency is consistent with an ester linkage to the surface [typically 1,720–1,760 cm^{-1} (23)]. Forming a bond to the silicon surface imparts significant stability to the monolayers. They were able to survive rinsing or soaking in common solvents such as THF and methylene chloride.

Surface x-ray reflectivity is in agreement with the UV-visible (UV-vis) experiments indicating that the molecules are essentially upright on the surface and tightly packed (24, 25). Fig. 3*C* shows the x-ray reflectivity for **1B** on the surface of silicon oxide. The reflectivity can be fit well by using the Parratt formalism to a box model with three layers: a silicon oxide layer, an ester layer, and a hexa-kata-benzocoronene (HBC) core layer (26). The fit yields a monolayer thickness of ≈12.4 Å, composed of the ester layer and the HBC core, suggesting that the monolayer is essentially upright on the surface of silicon oxide. A real-space electron-density profile showing the deconvolution into three regions (along with their corresponding electron densities) is shown in Fig. 3*D*. A color-coded model of the three layers is shown in Fig. 3*E*. A striking result from the x-ray scattering is the extremely high electron density (0.54 $e^-/Å^3$) for the HBC layer. The theoretical electron density for the HBC is 0.55 $e^-/Å^3$, much higher than other monolayers of organic semiconductors (2). The tight packing of these molecules and their high π-electron density are a harbinger for the useful electronic properties described below.

The monolayers are π-stacked as implied by the IR, UV-vis, and surface x-ray scattering mentioned above and confirmed by the photoluminescence of the monolayers on silicon oxide surfaces. Fig. 3*B* shows a comparison of photoluminescence spectra from a monolayer and a dilute solution of **1B**. There is a broad tail on the emission and significant red-shifting when the monolayer spectrum is compared with that from solution. This type of shift is a hallmark of aggregation in disk-shaped molecules due to delocalization of the excited state (19).

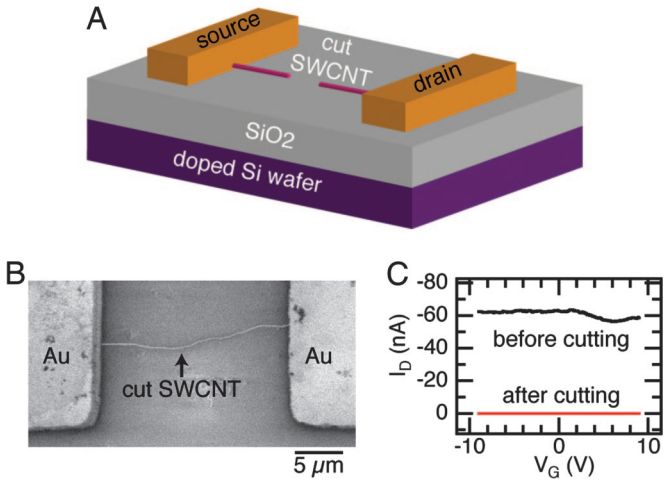

Fig. 2. The electrodes are formed by cutting an individual, metallic SWNT. (*A*) A cut SWNT on a doped silicon wafer contacted by large metal pads. The cut nanotube serves as the S/D electrodes, and the silicon wafer acts as the global back-gate for the device. (*B*) SEM micrograph of an individual SWNT between gold electrodes after being oxidatively cut. (*C*) Electrical properties (I_D vs. V_G at $V_D = -50$ mV) of a metallic tube before (black trace) and after (red trace) oxidative cutting.

Electrical Testing. We use the nanotube electrodes described above to probe the electrical properties of these monolayers. To form the devices, we immerse the open nanotube circuits (Fig. 2) in a THF solution of **1B** or **1C** (with pyridine added to scavenge the HCl). The devices were removed from solution, rinsed, and dried under a stream of inert gas. Monolayers of both **1B** and **1C** behave as *p*-type semiconducting films. Fig. 4 shows the transistor characteristics for a monolayer of **1C** assembled in the very same device characterized in Fig. 2*C*. These devices can be cycled many times despite the high levels of current within these self-assembled stacks. Similar data are available for **1B** in Fig. 7, which is published as supporting information on the PNAS web site, although the devices from **1B** had a qualitatively shorter lifetime under the conditions of the measurement.

To ensure that the current path was through the nanotube electrodes and not through the macroscopic gold contacts, we tested devices with only the metal electrodes, lacking the nanotube. All of these devices behaved as open circuits with no field effect induced by the gate electrode. Because the diameter of these self-assembled columns (≈2.8 nm for **1C** with its side chains fully extended) is larger than the diameter of a typical SWNT (≈1–2 nm), the maximum number of columns that these nanotube electrodes can contact is two, even considering significant fringing fields near the electrodes. Given the size of the gap and the volume of the molecules assembled in this gap, we can estimate that the collective properties of ≈4–12 molecules are being probed (assuming that the molecule pack is ≈0.5 nm, face-to-face, and is ≈2.5 nm in diameter) (19). To further understand the importance of the contact material and geometry, we fabricated devices with gaps between platinum electrodes. These electrodes were much wider (≈30 nm), but the

CHEMISTRY

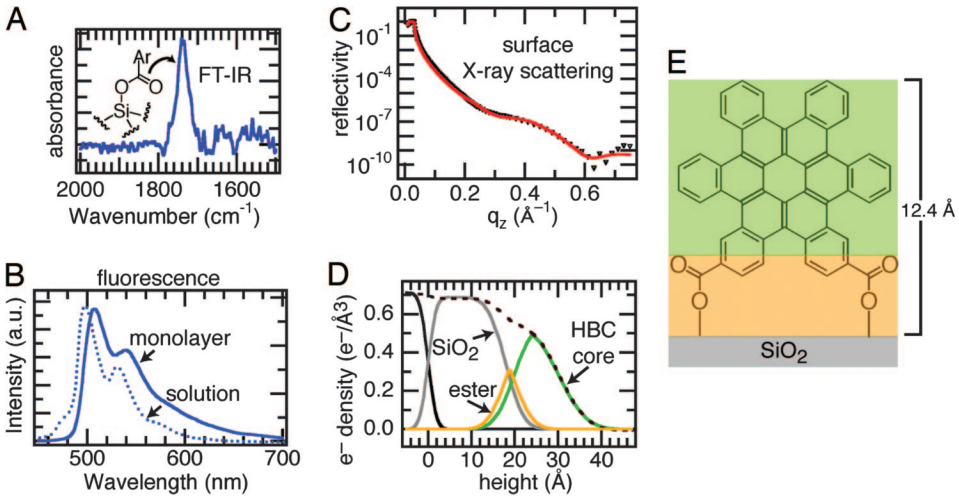

Fig. 3. The HBCs form dense, upright monolayers on the surface of silicon oxide. (*A*) Carbonyl region of the FTIR spectrum of a silicon wafer after reaction with **1B**. (*B*) Comparison of solution (6.4×10^{-6} M in THF) and monolayer fluorescence emission of **1B** (excitation at 385 nm). (*C*) Surface x-ray scattering of **1B**. Data, black triangles; fit to a three-layer model (red line). (*D*) Real-space model of the fit from *C* showing the deconvolution of the electron density into three layers: silicon oxide, ester, and HBC. (*E*) Model with three layers color-coded to the real-space model.

gaps between them were small (between 3 and 10 nm) (27). Micrographs of these devices are contained in Fig. 8, which is published as supporting information on the PNAS web site. There was no measurable switching or conductance in 120 devices of this type that were tested.

Chemoresponsive Properties. Because the active channel of the monolayer device prepared here is exposed and available for recognition, they are sensitive to certain types of molecules (28–31). Fig. 4 *C* and *D* shows the transistor characteristics for the same device shown in Fig. 4 *A* and B after dipping into a solution of the well known electron acceptor TCNQ. Given the affinity of TCNQ for the molecules such as coronene (32), it likely acts as a dopant for the stacks by accepting π-electrons through charge transfer between the electron-deficient TCNQ and the electron-rich HBC. This result would explain the shift in voltage threshold to more positive values and why the OFF-current becomes higher by ≈1 order of magnitude. An uncut metallic SWNT device showed no effect when dipped into a solution of TCNQ, indicating that the change observed in Fig. 4 *C* and *D* is due to the interaction of TCNQ with the molecular stacks (see Fig. 9, which is published as supporting information on the PNAS web site). What is left unclear, however, is how this doping occurs whether it is through an intercalation of the TCNQ or another associative mechanism.

It is remarkable to note that these molecular transistors, which use the nanogap SWNT electrodes, exhibit ON/OFF current ratios as high as bulk OFETs (≈5 orders in Fig. 4). This ratio is one of the critical parameters for the success of OFETs and has proven difficult to optimize in ultrasmall devices prepared with

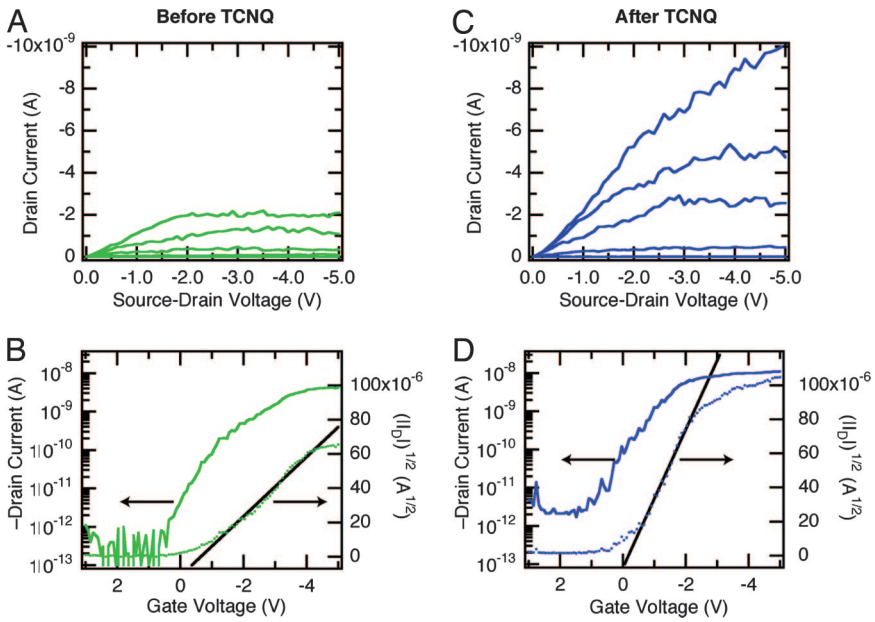

Fig. 4. Same device measured in Fig. 2*C* after the assembly of a monolayer of **1C** on the SiO_2 surface of a silicon wafer with a SWNT electrodes. (*A*) Transistor output, $V_G = 0$ to -5 V in 1-V steps. (*B*) Transfer characteristics for the device, $V_D = -2$ V. (*C*) Transistor output, $V_G = 0$ to -5 V in 1-V steps, for the same device measured in *A* after treatment with a TCNQ solution (1×10^{-3} M in CH_2Cl_2). (*D*) Transfer characteristics for the device, $V_{SD} = -2$ V.

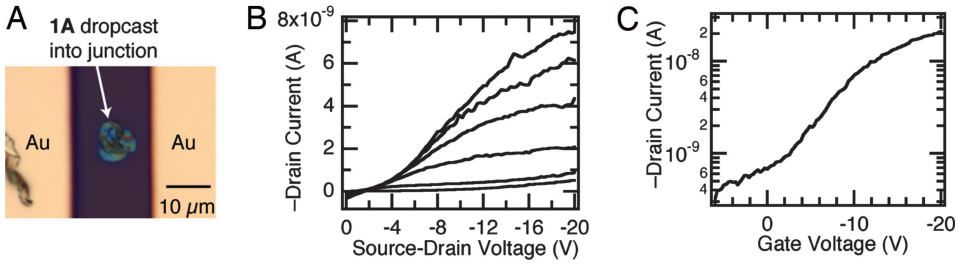

Fig. 5. Without the surface attachment, the device characteristics are poor. (*A*) Optical micrograph of a solution of **1A** drop cast into a gap formed from SWNT electrodes. (*B*) Transistor output for **1A** drop cast into a SWNT gap. The gate voltage ranges from 0 to −20 V in 4-V steps. (*C*) Transfer characteristics for **1A** drop cast into the SWNT gaps, $V_{SD} = -20$ V.

metallic S/D electrodes (3,4). In general, for nanoscale OFETs formed from metallic electrodes separated by only a few nanometers, the transistor characteristics suffer from inefficient field effect in the channel region of the device because of a screening of this field from the large metallic S/D electrodes. In these cases, the drain potential is dominant over the channel potential, providing inefficient device switching and a poor ON/OFF ratio. On the contrary, our monolayer OFETs with SWNT electrodes overcome these short channel effects. Owing to their 1D nature, the SWNT S/D electrodes screen the gate electric field only in proximity to the SWNT/junction regions (≈1 nm in lateral range). In such devices, the electric field from the back gate can efficiently penetrate into the middle of the channel where electrostatic band shifting enables the observed high ON/OFF ratio. Similar highly efficient device switching has been reported in other devices employing 1D SWNT electrodes (13, 14).

We also note that, in addition to the high ON/OFF ratio described above, the monolayer OFETs with SWNT contacts exhibit a sharp saturation of the drain current as the S/D bias (V_{SD}) increases. Fig. *4* A and *C* display I_D saturation for bias voltage as small as $V_{SD} = -2$ V. Typical devices made from organic thin film materials require much higher voltages, well over an order of magnitude higher. We suggest that the electrostatics of these 1D contacts in combination with the monolayer molecular conformation within the SWNT S/D gaps yields the observed highly efficient OFET behavior with relatively low S/D voltage. The 1D SWNT electrodes yields a sharply focused drain field in the channel region of the monolayer OFET to create a "pinch-off" to saturate the drain current. This result indicates that the conformational arrangement of the molecules conferred from the attachment is playing an important role here.

To test the relative importance of the electrostatics and surface attachment to the enhancement in the gate efficiency, we made devices by using molecules that lack functionality for attachment to the gate dielectric. For this process, we used the columnar mesogen **1A** to bridge the nanogaps between SWNTs. We have previously shown that **1A** forms efficacious thin film transistors when cast from solution (19). A small volume of solution of **1A** was drop cast so that it covered the junction in the SWNT but did not span the gold contact pads, shown in Fig. 5*A*. This device also shows *p*-type hole-transporting semiconductor behavior (Fig. 5 *B* and *C*). The device in Fig. 5 with unattached molecules requires nearly an order of magnitude greater gate bias to turn the devices ON when compared with the monolayer sample in Fig. 4. We infer from this result that the surface attachment is critical. The relevant physical picture for why there is such a large effect results from a confluence of factors. The upright conformation is enforced by the double attachment, and this conformation is synergistic with the molecules' propensity to stack laterally into columns with good π-overlap. Moreover, this arrangement is ideally suited to the 1D electrode geometry with its ability to focus the field into the channel.

There are only a few examples of organic semiconductors that have been measured with SWNT gaps, and they use crystallites of pentacene and an oligothiophene (14). The subthreshold swing (S) in the device in Fig. 4 *C* and *D* is ≈500 mV/decade and is similar to the values obtained by Dai and coworkers (14). Despite this similarity, the devices here turn on at considerably lower gate electric field because they use a much thicker silicon oxide layer (300 vs. 10 nm). This finding further highlights how efficiently the gate electrode is modulating the switching. The drain current saturation seen in Fig. 4 even at high S/D bias voltage has not been observed in the OFETs formed in between SWNT electrodes (14). Finally, the carrier mobility (≥1 $cm^2/V{\cdot}s$) is also very high. The mobility is only for comparison with other thin film devices because it assumes a parallel capacitor model for the gate dielectric, which is not accurate here. The mobility is calculated from the linear fit of $|I_{DS}|^{1/2}$ vs. $|V_G|$ shown in Fig. 4 (solid line) by using the equation $I_{DS} = (\mu WC_i/2L)(V_G - V_T)^2$ where $C_i = 11 \times 10^{-9}$ F, $W = 1.5$ nm, and $L = 3$ nm. The S/D voltage is set at −2 V.

It is not just the desirable device properties that make this approach useful; its value also has to do with the manyfold advantage of using self-assembled monolayers compared with crystals or evaporated thin films. Self-assembly allows for a simple, solution-based method for forming the active layer that can be patterned. Moreover, the covalent attachment also allows the devices to be immersed in liquids to allow testing of dopants and the formation of new types of sensors, such as in Fig. 4 with TCNQ. The surface atoms used to attach the molecular semiconductors dictate the orientation of the molecular semiconductors and therefore should provide a new means to tune and optimize carrier mobility. Finally, and most importantly, the top surface of the transistor's active layer is exposed, which renders them sensitive to their environment (Fig. 4 *C* and *D*) and charts a clear path to complex, layer-by-layer assemblies.

Conclusions

This work is a stark example of how the ever-reducing dimensions of top-down device fabrication can be tailored to meet the ever-expanding length-scales of bottom-up self-assembly. It highlights the possibility to use synthesized interfaces and nanostructures as a means to tailor electrical devices and points to a very different method to create materials. These devices, although still not optimized, require very low gate bias for switching (33). Because the channel of these monolayer devices is exposed, they are responsive to their chemical environment. These chemoresponsive devices should have broad utility as ultrasensitive devices for environmental and chemical sensing.

Materials and Methods

Synthesis. Compounds **1B** and **1C** were synthesized by a procedure that is similar to the one developed for **1A** (19). Full characterization is provided in *Supporting Materials and Methods*, which is published as supporting information on the PNAS web site.

SWNT Device Preparation/Characterization. Devices were made from individual SWNTs that were grown by using chemical vapor deposition by a procedure that has been described (13). These devices then were oxidatively cut by using high-resolution electron-beam lithography and an oxygen plasma (13). These devices were electrically tested by using a standard semiconductor parameter analyzer and probe station.

Monolayer Formation. The monolayer assemblies were prepared on silicon wafers (Addison Engineering), or quartz flats (NSG Precision Cells) that were used for the spectroscopy. We initially cleaned the silicon oxide surfaces by soaking them in dichloromethane at room temperature for 15 min, followed by 20 min in an SC1 solution (5:1:1 deionized H_2O:NH_4OH:H_2O_2) at 70°C. They then were rinsed in deionized H_2O and dried in a stream of N_2 gas. Immediately after this cleaning procedure, the samples were immersed in a saturated solution of **1B** or $\approx 10^{-4}$M solution of **1C** in ≈30 ml of THF, with 0.5 ml of pyridine at room temperature overnight. After functionalization, the samples were washed three times with THF.

UV-Vis Spectroscopy. We used UV-vis spectroscopy to determine the monolayer density on thin quartz substrates, to reduce background contributions. The spectrometer used for these experiments was a single-beam Agilent 8543 spectrophotometer, with a modified sample holder for thin film measurements.

Fluorescence Spectroscopy. Photoluminescence spectra were taken with a Jobin Yvon Fluorolog-3 Spectrofluorometer (Model FL-TAU3) on a silicon wafer with a native oxide layer. The system has a photomultiplier tube (PMT) detector and a Xe source. We mounted the samples at a 45° angle and collected their emission in front-face mode. The samples were excited at the wavelength of maximum absorption (385 nm), and the integration time was 2 s.

Reflection–Absorption IR Spectroscopy. Reflection–absorption IR spectroscopy was performed by using a N_2-purged Nicolet IR spectrometer with a mercury cadmium tellurium (MCT) detector. Spectra were obtained by using a GATR (Harrick Inc.) total reflectance accessory equipped with a hemispherical germanium crystal.

Surface X-Ray Reflectivity. X-ray reflectivity was performed by using a described setup (24, 25).

We thank Ben Ocko for assistance with the x-ray measurements and Limin Huang and Stephen O'Brien for assistance in the growth of the SWNT. This work was supported by National Science Foundation (NSF) Nanoscale Science and Engineering Initiative Award CHE-0117752; the New York State Office of Science, Technology, and Academic Research (NYSTAR); and Department of Energy Nanoscience Initiative NSET#04ER46118. C.N. was supported by NSF CAREER Award DMR-02-37860, the Camille Dreyfus Teacher Scholar Program (2004), and the Alfred P. Sloan Fellowship Program (2004). This work also was supported in part by NSF Materials Research Science and Engineering Center Program Award DMR-0213574 and by NYSTAR (to M.L.S. and the shared instrument facility). J.B. was supported by Department of Energy Division of Materials Science Contract DE-AC02-98CH10886.

1. Kagan, C. R., Afzali, A., Martel, R., Gignac, L. M., Solomon, P. M., Schrott, A. G. & Ek, B. (2003) *Nano Lett.* **3,** 119–124.
2. Tulevski, G. S., Miao, Q., Fukuto, M., Abram, R., Ocko, B., Pindak, R., Steigerwald, M. L., Kagan, C. R. & Nuckolls, C. (2004) *J. Am. Chem. Soc.* **126,** 15048–15050.
3. Dimitrakopoulos, C. D. & Malenfant, P. R. L. (2002) *Adv. Mater.* **14,** 99–117.
4. Kagan, C. R. & Andry, P. (2003) *Thin-Film Transistors* (Dekker, New York).
5. Dodabalapur, A., Torsi, L. & Katz, H. E. (1995) *Science* **268,** 270–271.
6. Sandberg, H. G. O., Frey, G. L., Shkunov, M. N., Sirringhaus, H., Friend, R. H., Nielsen, M. M. & Kumpf, C. (2002) *Langmuir* **18,** 10176–10182.
7. Horowitz, G. (1998) *Adv. Mater.* **10,** 365–377.
8. Murphy, A. R., Chang, P. C., VanDyke, P., Liu, J., Frechet, J. M. J., Subramanian, V., DeLongchamp, D. M., Sambasivan, S., Fischer, D. A. & Lin, E. K. (2005) *Chem. Mater.* **17,** 6033–6041.
9. Ruiz, R., Papadimitratos, A., Mayer, A. C. & Malliaras, G. G. (2005) *Adv. Mater.* **17,** 1795–1798.
10. Miyazaki, T., Kobayashi, K., Ishida, K., Hotta, S., Horiuchi, T., Matsushige, K. & Yamada, H. (2005) *J. Appl. Phys.* **97,** 124503/1–124503/4.
11. Heim, T., Lmimouni, K. & Vuillaume, D. (2004) *Nano Lett.* **4,** 2145–2150.
12. Huang, L., Cui, X., White, B. & O'Brien, S. P. (2004) *J. Phys. Chem. B* **108,** 16451–16456.
13. Guo, X., Small, J. P., Klare, J. E., Wang, Y., Purewal, M. S., Tam, I. W., Hong, B. H., Caldwell, R., Huang, L., O'Brien, S., *et al.* (2006) *Science* **311,** 356–359.
14. Qi, P. F., Javey, A., Rolandi, M., Wang, Q., Yenilmez, E. & Dai, H. J. (2004) *J. Am. Chem. Soc.* **126,** 11774–11775.
15. Tsukagoshi, K., Yagi, I. & Aoyagi, Y. (2004) *Appl. Phys. Lett.* **85,** 1021–1023.
16. Appenzeller, J., Knoch, J., Radosavljevic, M. & Avouris, P. (2004) *Phys. Rev. Lett.* **92,** 226802/1–226802/4.
17. Dai, H. (2002) *Acc. Chem. Res.* **35,** 1035–1044.
18. Tans, S. J., Verschueren, A. R. M. & Dekker, C. (1998) *Nature* **393,** 49–52.
19. Xiao, S., Myers, M., Miao, Q., Sanaur, S., Pang, K., Steigerwald, M. L. & Nuckolls, C. (2005) *Angew. Chem. Int. Ed.* **44,** 7390–7394.
20. Ulman, A. (1996) *Chem. Rev.* **96,** 1533–1554.
21. Schreiber, F. (2000) *Prog. Surf. Sci.* **65,** 151–256.
22. Onclin, S., Ravoo, B. J. & Reinhoudt, D. N. (2005) *Angew. Chem. Int. Ed.* **44,** 6282–6304.
23. Nakanishi, K. & Solomon, P. H. (1977) *Infrared Absorption Spectroscopy* (Holden–Day, San Francisco).
24. Baptiste, A., Gibaud, A., Bardeau, J. F., Wen, K., Moaz, R., Sagiv, J. & Ocko, B. M. (2002) *Langmuir* **18,** 3916–3922.
25. Gibaud, A. (1999) *X-ray and Neutron Reflectivity: Principle and Applications* (Springer, Paris).
26. Parratt, L. G. (1954) *Phys. Rev.* **95,** 359–369.
27. Tang, J., De Poortere, E. P., Klare, J. E., Nuckolls, C. & Wind, S. J. (2006) *Microelectron. Eng.* **83,** 1706–1709.
28. Torsi, L. & Dodabalapur, A. (2005) *Anal. Chem.* **77,** 380A–387A.
29. Liao, F., Chen, C. & Subramanian, V. (2005) *Sensors Actuators B* **107,** 849–855.
30. Yamagishi, Y., Ise, M., Takano, N. & Fukuda, H. (2004) *Chem. Sensors* **20,** 704–705.
31. Crone, B., Dodabalapur, A., Gelperin, A., Torsi, L., Katz, H. E., Lovinger, A. J. & Bao, Z. (2001) *Appl. Phys. Lett.* **78,** 2229–2231.
32. Chi, X., Besnard, C., Thorsmolle, V. K., Butko, V. Y., Taylor, A. J., Siegrist, T. & Ramirez, A. P. (2004) *Chem. Mater.* **16,** 5751–5755.
33. Halik, M., Klauk, H., Zschieschang, U., Schmid, G., Dehm, C., Schuetz, M., Maisch, S., Effenberger, F., Brunnbauer, M. & Stellacci, F. (2004) *Nature* **431,** 963–966.